Integrated FDI and Control for Transport Aircraft

Andrés Marcos [*] , Gary J. Balas [†] and József Bokor [‡]

It is known that the robust integrated design of the controller and the diagnosis filter for a system has several advantages with respect to their independent designs. In this paper an application of the integrated controller / diagnosis filter using $\mathcal{H}_\infty$-optimization techniques to a nonlinear system, the longitudinal motion of a Boeing 747-100/200 aircraft, is presented. The integrated design formulation (interconnection and weight selection) is carried out for five LTI plants obtained through out the Up-and-Away flight envelope. Closed-loop time simulations are carried out using the LTI plants and the full nonlinear equations of motion of the aircraft, longitudinal and lateral, under a realistic turbulence and noise environment.

I. Introduction

The integrated design of the controller and fault diagnosis & identification (FDI) filter for a system with uncertainty is known to have several advantages with respect to their independent design. Specifically, the trade-off between the controller and the filter (i.e. the robustness of the controller vs. the performance of the filter) can be addressed directly in the integrated case. Also, the integrated design allows to directly synthesize the controller to tolerate faults.

The controller / filter trade-off has been analyzed in references.[1–3] Intuitively, this trade-off is easily understood for the case of a highly robust controller. A controller of this type will hide the effects of the faults since they are treated as disturbances, constraining the performance of the FDI filter. To address this trade-off a number of approaches have been proposed in the literature. In reference[1] an integrated control / filter approach was proposed and the opposing objectives qualitatively analyzed. This integrated approach was casted in a general framework and solutions, based on optimal and robust theory, were proposed in reference.[4] The previous two references were further developed in[2] which proposed solutions in terms of the standard robust control configuration[5] for nominal and uncertain systems. In reference,[3] a mixed $\mathcal{H}_2/\mathcal{H}_\infty$ criterion was used to design a reconfigurable control with optimized control and diagnostic performance indexes.

From a different perspective, the Youla and the Dual Youla parameterizations were studied for high-performance controllers in reference.[6] A main result from this reference is that there is also a separation principle for this type of controllers. In that same reference, nested structures based on both parameterizations were studied to improve the performance of the controller. This high-performance controller separation principle and its connections with the residual generation theory have been used recently in a breadth of papers proposing different architectures for the controller and the diagnostic filter design, see.[7–9]

The focus of this paper is on the application of the integrated controller / diagnosis filter design using $\mathcal{H}_\infty$-optimization techniques to a nonlinear system, the longitudinal motion of a Boeing 747-100/200 aircraft model. The integrated design formulation (interconnection and weight selection) is carried out using LTI plants obtained at five equilibrium points through out the Up-and-Away flight envelope of the Boeing 747-100/200 aircraft. The same interconnection structure and weights are used for all the LTI models in order to assess the robustness of the designs and the possibility of gain-scheduling the five LTI integrated controllers to cover the entire flight envelope. Closed-loop time simulations are carried out using the LTI plants and the full nonlinear equations of motion of the aircraft, longitudinal and lateral, under a realistic turbulence and noise environment.

The layout of the paper is as follows. Section II briefly introduces background theory. The linear and nonlinear models are described in Section III. Section IV presents the problem formulation and objectives for the integrated design. The analysis of the resulting designs is presented in Section V. These analyses include sensitivity analysis, and linear and nonlinear time simulations for several fault cases. The conclusions are given in Section VI.

[*]Post-Doctoral Fellow at the University of Leicester, Dept. of Engineering, e-mail: ame12@leicester.ac.uk

[†]Professor, University of Minnesota, Department of Aerospace Eng. and Mechanics, e-mail:balas@aem.umn.edu

[‡]Professor, Hungarian Academy of Sciences, Computer and Automation Research Institute, e-mail: bokor@sztaki.hu

II. Theory

In this section a review of the integrated controller / FDI filter approach is presented. This approach relies on the Youla parameterization and was first developed by C.N. Nett[1,10] with the so-called four-parameter controller. The four-parameter controller is a generalization of the Youla parameterization which extends the controller to four degrees of freedom (DoF) by considering the generation of a diagnostic signal. The four DoF are associated with reference signal tracking, closed-loop stabilization, residual generation, and disturbance rejection. Figure 1 shows the structure for the parameterization of all 4-parameter controllers given a system $G \in \mathcal{R}_P$ (the space of real-rational, and proper functions), the general result is formalized in Theorem II.1:

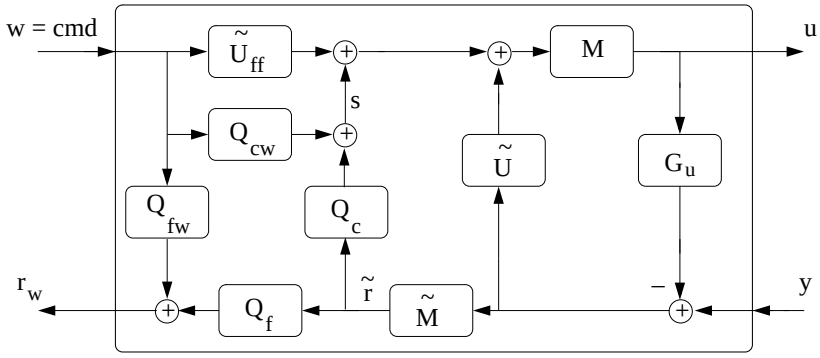

Figure 1. Four-parameter controller parameterization structure.

Theorem II.1 (General Four-parameter Controller) *Consider a nominal plant $G_u \in \mathcal{R}_P$. Assume a corresponding nominal stabilizing controller, $K_o \in \mathcal{R}_P$, and feedforward controller, $K_{ff} \in \mathcal{R}_P$, are given. Let any right coprime factorization (r.c.f.) and left coprime factorization (l.c.f.) for the nominal plant, $G_u = N_u M^{-1} = \tilde{M}^{-1}\tilde{N}_u$, and the controllers, $K_o = UV^{-1} = \tilde{V}^{-1}\tilde{U}$ and $K_{ff} = U_{ff}V^{-1} = \tilde{V}^{-1}\tilde{U}_{ff}$, be known. The class of all proper integrated (stabilizing and residual generator) controllers $K_F(Q) \in \mathcal{R}_P$ is parameterized by:*

$$\begin{bmatrix} u \\ r_w \end{bmatrix} = \begin{bmatrix} (\tilde{V}+Q_c\tilde{N}_u)^{-1}(\tilde{U}+Q_c\tilde{M}) & (\tilde{V}+Q_c\tilde{N}_u)^{-1}(\tilde{U}_{ff}+Q_{cw}) \\ Q_f\left(\tilde{M}-\tilde{N}_u(\tilde{V}+Q_c\tilde{N}_u)^{-1}(\tilde{U}+Q_c\tilde{M})\right) & Q_{fw}-Q_f\tilde{N}_u(\tilde{V}+Q_c\tilde{N}_u)^{-1}(\tilde{U}_{ff}+Q_{cw}) \end{bmatrix} \begin{bmatrix} y \\ w \end{bmatrix} \tag{1}$$

Under the following conditions:

$$\begin{bmatrix} s \\ r_w \end{bmatrix} = Q \begin{bmatrix} \tilde{r} \\ w \end{bmatrix} = \begin{bmatrix} Q_c & Q_{cw} \\ Q_f & Q_{fw} \end{bmatrix} \begin{bmatrix} \tilde{r} \\ w \end{bmatrix} \in \mathcal{RH}_\infty, \qquad (\tilde{V}+Q_c\tilde{N}_u)(\infty) \text{ exist} \tag{2}$$

The controller output vectors are the feedback control input u and the residual vector r_w; the controller input vectors are the plant measurements y and the exogenous input $w = cmd$. The internal signals s and $\tilde{r}$ are respectively the contribution of the Youla parameters to the feedback controller and the primary residual.

Proof: The proof based on Theorem (33) in reference[10] and Theorem 12.17 from[5] can be obtained in reference.[11]

Remark 1. In this parameterization a feedforward controller, $K_{ff} = \tilde{V}^{-1}\tilde{U}_{ff}$, is included. The coprime factor $\tilde{V}$ has been assumed common for both controller terms due to the well-known requirement that K_{ff} be stable or if unstable, implemented together with the feedback controller $K = \tilde{V}^{-1}\tilde{U}$. Note that in Figure 1 the term $\tilde{V}$ is not shown, but it can be obtained by performing algebraic manipulations on equation (1).

Remark 2. The controller parameterization of equation (1) is an adaptation, but equivalent (after setting $\tilde{U}_{ff} = 0$ and performing direct algebraic manipulations), to the formulae given in.[1,10] It is observed in Figure 1 that the class of four-parameter controllers is associated with the implicit internal model principle, i.e. the parameterization contains a model of the plant. This association is highlighted by the internal signal $\tilde{r}$ which is called the primary residual and is equal to:

$$\tilde{r} = \tilde{M}y - \tilde{N}_u u \tag{3}$$

From this primary residual signal it is also easy to see the connection with the residual generation theory. The parameterization of all residual generators for a system $y = G_u\ u + G_d\ d + G_f\ f$ can be given in terms of a free-parameter $Q_f \in \mathcal{RH}_\infty$, see.[12,13] Introducing the fault and disturbance signals $[f^\top\ d^\top]^\top$, the residual vector r can be generated using the following frequency-domain residual generator:

$$r = Q_f\ \tilde{r}\ =\ Q_f\ (\tilde{M}\ y - \tilde{N}_u\ u) = Q_f\ (\tilde{N}_f\ f + \tilde{N}_d\ d) \tag{4}$$

Note that for the nominal case, the residual generator cancels the effect of the inputs to the monitored system. The different FDI approaches are basically based on the diverse ways available to select the transfer functions $Q_f, \tilde{N}_f, \tilde{N}_d$ such that conditions on detectability, isolability, identification of faults, and filter performance are fulfilled, see reference.[14] Also, notice that in the general case of the four-parameter controller the diagnostic signal r_w equals the residual from equation (4) corrected by a term due to the exogenous input influence, i.e. $(Q_{fw}\ w)$.

Remark 3. Removing the second row in the controller, corresponding to the diagnostic signal generation, the standard two degree-of-freedom controller parameterization from[15] is obtained. Furthermore, the controller term K_{11} corresponds to the one degree-of-freedom Youla parameterization. A detailed analysis of the transfer function constraints and algebraic limitations with respect to nominal performance, robust stability and other closed-loop properties for the integrated approach is given in references.[1,2,16,17]

In reference,[2] the above general parameterization is studied from the perspective of an integrated two DoF design (i.e stabilizing controller with diagnostic signal generation properties). That reference also provides an in-depth study of the adequacy of the integrated approach versus the independent design of the controller and filter. The result obtained in that reference is that there is a separation principle for the nominal case that is not present for the uncertain case. These studies lead to the conclusion that for the uncertain case it is more advantageous to design the controller and the fault detection filter within an integrated framework to better trade-off the filter performance and the controller robustness.

III. Models and Environment

In this section the aircraft nonlinear and linear time-invariant (LTI) models for the longitudinal axis and the turbulence and sensor models are presented. A more detailed presentation of the nonlinear aircraft model can be found in references.[18,19] The LTI longitudinal motion models are used in the design stage while the full nonlinear model is used in the nonlinear simulations to assess the robustness and performance of the designed integrated controller with the actual model.

The aircraft model used for this application is the Boeing 747 series 100/200. The Boeing 747 aircraft is an intercontinental wide-body transport with four fan jet engines designed to operate from international airports. The focus of the application is on the longitudinal motion of the aircraft. A movable horizontal stabilizer with four elevator segments (i.e. two inboards and two outboards) and the four engines thrust are used to control the longitudinal axis motion. The horizontal stabilizer, δ_s is only used for trimming purposes. Assuming normal operation of the aircraft, the inboard and outboard elevators move together, hence for our purposes the model will be assumed to have one elevator surface, δ_e.

An accurate representation of the dynamics of an aircraft can be obtained through nonlinear, rigid body equations (note, that in this case the flexible modes are ignored). References[20,21] provide complete derivations of the rigid body equations for an airplane. The nonlinear body-axes longitudinal motion of the Boeing 747, not including flexible effects, can be described by the following differential equations:

$$\dot{\alpha} = \frac{[-F_x\ s_\alpha + F_z\ c_\alpha]}{m\ V_{TAS}} + q \tag{5}$$

$$\dot{q} = c_7\ M_y \tag{6}$$

$$\dot{\theta} = q \tag{7}$$

$$\dot{V_{TAS}} = \frac{1}{m}\ [F_x\ c_\alpha + F_z\ s_\alpha] \tag{8}$$

$$\dot{he} = V_{TAS}\ c_\alpha\ s_\theta - V_{TAS}\ s_\alpha\ c_\theta\ =\ V_{TAS}\ sin\gamma \tag{9}$$

The longitudinal states are angle of attack α (rad), pitch rate q (rad/s), true velocity V_{TAS} (m/s), pitch angle θ (rad), and altitude *he* (m). The aerodynamic forces along the X and Z-axis and the pitching moment are given by F_x, F_z and M_y respectively. The inertial coefficient is given by $c_7 = 1/I_{yy}$ (1/Kg/m^2) and the cosine and sine by c_α and s_θ. The aerodynamic forces and moments are defined in terms of dimensionless aerodynamic coefficients ($C_D, C_L, C_Y, C_l, C_m, C_n$), flight dynamic pressure $\bar{q}\ (N/m^2)$, reference area $S\ (m^2)$, and in the case of the moments, the moment-arm (either wing chord $\bar{c}$ (m), or wing span b (m)). The aerodynamic coefficients are provided as look-up tables (LUT) function of a wide set of parameters (angle of attack, true airspeed, sideslip angle, and altitude among others). The reduced aerodynamic coefficients used in references[11,22] are also used in this case.

LTI plant models are used for design of the integrated controllers. They are obtained through Jacobian linearisations of the nonlinear model at different points in the flight envelope of interest (*he* $\in$ [4000,10000] m, $Vtas \in$ [150,250] m/s). Table 1 shows the five trim points in the flight envelope used for design.

point	altitude, m	airspeed, m/s	Mach number
1	4000	184	0.567
2	4000	232	0.71
3	9250	215.5	0.71
4	9250	247.75	0.81
5	7000	241	0.77

Table 1. Trim points.

The LTI models have five states : pitch rate q (rad/s), true airspeed V_{TAS} (m/s), angle-of-attack α (rad), pitch angle θ (rad), and altitude *he* (m). There are two control inputs: elevator deflection δ_e (rad) and the combined thrust for the four engines Tn (N). The measurements available are flight path angle γ (rad), normal acceleration in g's $\dot{V}/g$ (non-dim), pitch angle θ (rad), pitch rate q (rad/s), velocity V_{TAS} (m/s), and altitude *he* (m).

The deflection and rate limits for the elevator are -23 to 17 deg and ± 37 deg/s respectively, see reference.[23] Taking the rate limits into account, the elevator is modeled as simple first-order transfer functions: $act_{\delta_e} = 37/(s+37)$. The engine dynamics are modeled as $act_{eng} = 0.5/(s+0.5)$ based on the engine transient characteristics provided in reference.[23]

The closed-loop simulations are corrupted by noise in the sensors and by a turbulence model entering the nonlinear aircraft model through the stability derivatives. Turbulence is simulated by feeding white noise through stable, minimum-phase spectra filters to the system. There are several analytical functions which provide turbulence spectra[20,24] but the Dryden spectra model is the most common. For the longitudinal (symmetric) and lateral (asymmetric) motions of an aircraft in turbulence the model developed at Delft University of Technology is followed, see reference.[24] Coloring filters are used in the simulation to achieve a realistic level of noise in the sensor measurements. The sensor dynamics are modeled using low-pass filters.

IV. Integrated Controller/Filter Design

In this section the control and diagnosis objectives for the integrated design are presented together with the problem formulation and weight selection used to achieve them. The design of an $\mathcal{H}_\infty$-optimization controller is characterized by two basic steps: the selection of the interconnection (problem formulation) and the choice of appropriate weights (optimization objectives formulation). The integrated design, interconnection and weight selection, is carried out for five LTI plants obtained at five equilibrium points through out the Up-and-Away flight envelope of the Boeing 747-100/200 aircraft, see Table 1. The same interconnection structure and weights are used for all the LTI models in order to assess the robustness of the designs and the possibility of gain-scheduling the five LTI integrated controllers to cover the entire flight envelope.

The controller objectives are to achieve de-coupled tracking of flight path angle command γ_c and velocity command $Vtas_c$ with settling times of 15 sec and 45 sec respectively, see reference.[25] These performance characteristics are assuming fully functional elevator surfaces and sensors. Furthermore, the controller should be robust to model uncertainty and should reject gust disturbances for the Up-and-Away flight envelope. In the case of faults in the elevator actuator and/or pitch rate sensor, the controller should be able to maintain stability and for not too severe faults provide adequate performance. Hence, it is required to design a robust fault tolerant controller with good performance characteristics for the nominal case.

The diagnosis objectives are to detect and isolate failure signals for the elevator actuator and the pitch rate sensor with de-coupling from the commands, see reference.[22] The diagnostic channels should be robust to model uncertainty and plant variations, and should be able to reject or attenuate disturbances (gust, noise, ...).

A model-matching formulation is used to track the desired commands (velocity and flight path angle) and provide diagnostic of the desired faults (elevator and pitch rate sensor). Furthermore, the control objectives are achieved by using a two-degree controller formulation. The faults are assumed to enter the system in an additive manner: e.g. the elevator deflection to the plant δ_e is equal to the actuator deflection *Act* plus the fault f_{act}. The final interconnection is given in Figure 2.

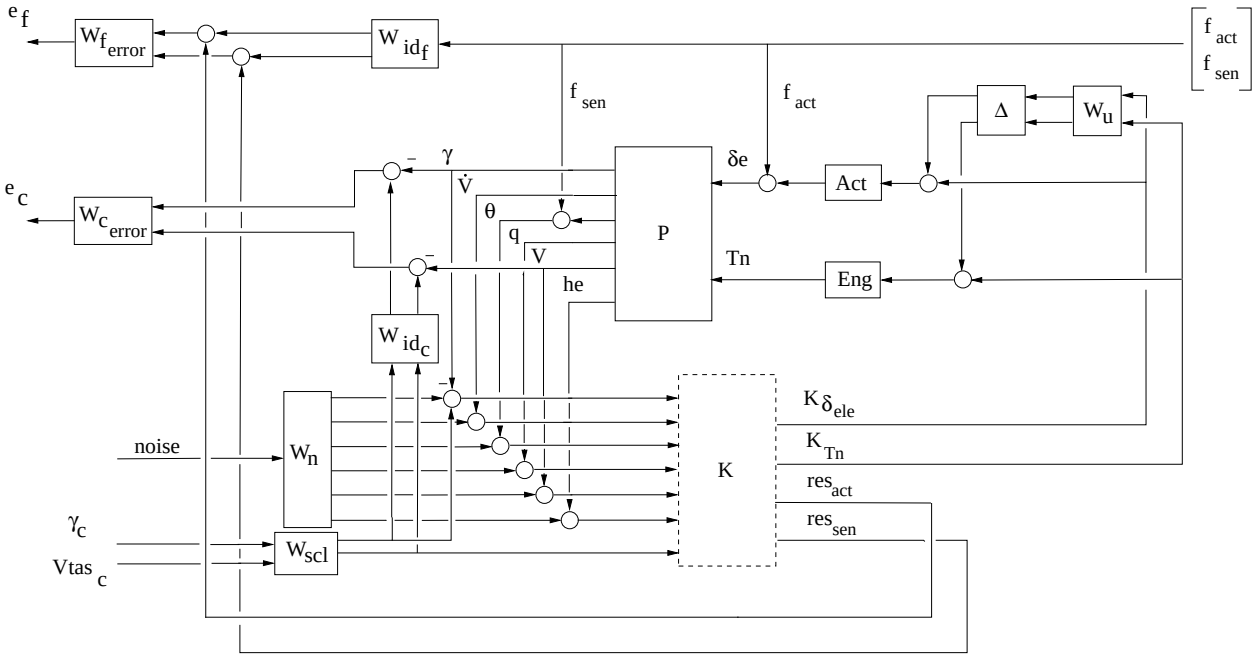

Figure 2. Integrated controller interconnection.

The exogenous inputs to the interconnection are the *noise* vector, the command signals $(\gamma_{cmd}, Vtas_{cmd})$, and the fault signals (f_{act}, f_{sen}). The interconnection outputs are the error channels for the control and the diagnosis objectives: $e_c = [\gamma_{error} \;\; Vtas_{error}]^\top$ and $e_f = [act_{error} \;\; sen_{error}]^\top$. The LTI plant outputs are flight path angle γ (deg), normal acceleration in g's $\dot{V}/g$ (non-dim), pitch angle θ (deg), pitch rate q (deg/s), true airspeed $Vtas$ (m/s) and altitude *he* (m). The plant inputs are the elevator deflection δ_e (deg) and the engine thrust Tn (Newtons). The disturbance vector is given by *noise* and consists of noise for each feedback channel. The integrated controller inputs are the difference between the flight path angle command and its output $(\gamma_{cmd} - \gamma)$, the rest of the plant outputs $(\dot{V}/g, \theta, q, Vtas, he)$, and the velocity command $Vtas_{cmd}$. The integrated controller outputs are four: two signals for feedback control, $K_{\delta_{ele}}$ and K_{Tn}, and two diagnosis signals, res_{act} and res_{sen}. There are two uncertainty input and output channels corresponding to $z = \Delta w$.

Since the formulation of the problem is based on model-matching, ideal models for the control and diagnosis signals are used. The ideal transfer function for the flight path angle response Wid_γ is modeled as a second-order system having a cut-off frequency at 0.35 rad/sec and a damping factor of 1, see equation (10). The settling time for this model is approximately 20 seconds (corresponding to a bandwidth of 0.22 rad/sec). For the ideal velocity model, a second-order model is also used with a settling time of 45 seconds. This is accomplished using a natural frequency of 0.15 rad/sec and the same damping factor as before to obtain a bandwidth of 0.1 rad/sec approximately, see equation (11). These ideal models are taken from reference.[25] An input scaling weight W_{scl} is used to normalize the command signals. The weight is selected as $diag(2,7)$ corresponding to 2 degrees of γ_{cmd} and 7 m/s for the $Vtas_{cmd}$.

$$Wid_{\gamma} = \frac{0.35^2}{s^2 + 2 \cdot 0.35 \cdot s + 0.35^2} \qquad Wid_{act} = 2\frac{\frac{s}{300}+1}{\frac{s}{2}+1} \tag{10}$$

$$Wid_{Vtas} = \frac{0.15^2}{s^2 + 2 \cdot 0.15 \cdot s + 0.15^2} \qquad Wid_{sen} = \frac{\frac{s}{300}+1}{s+1} \tag{11}$$

The ideal models for the faults are selected assuming a quite fast and reliable identification of the fault at low to mid range frequencies to avoid critical damage. Hence, the ideal model for the actuator fault Wid_{act} has a bandwidth around 2 rad/sec, corresponding to the faster dynamics of the actuator, while the sensor fault ideal model Wid_{sen} has a bandwidth of 1 rad/sec approximately.

Error weights are used to specify the performance objectives for the control $W_{c_{error}}$ and the diagnosis objectives $W_{f_{error}}$. These weights define the overall characteristics of the integrated controller: e.g. bandwidth requirements, steady-state requirements, and attenuation/amplification of signals at certain frequency ranges. The final selected weights are given by:

$$We_{\gamma} = \frac{\frac{s}{5}+1}{\frac{s}{0.1}+1} \qquad We_{act} = \frac{\frac{s}{5}+1}{\frac{s}{0.001}+1} \tag{12}$$

$$We_{Vtas} = 1.5\frac{\frac{s}{100}+1}{\frac{s}{0.05}+1} \qquad We_{sen} = \frac{\frac{s}{10}+1}{\frac{s}{0.1}+1} \tag{13}$$

The performance error weights for the control objectives We_{γ} and We_{Vtas} are scaled back at the output by the inverse of the scaling weight W_{scl} in order to preserve the input-output relation (this inverse weight is embedded in $W_{c_{error}}$ in Figure 2).

An input multiplicative uncertainty model is used to improve the robustness characteristics of the design. Typically, these uncertainty weights are used to limit the controller bandwidth and allow for increasing model error at higher frequencies. In this formulation, a constant uncertainty weight provided sufficient uncertainty and reduced the number of states of the interconnection (and hence of the final integrated controller). Wu is a diagonal weight, one channel for each plant input, both constants of 0.1 magnitude corresponding to 10 percent uncertainty.

The last weights in the interconnection correspond to output disturbances. These weights are used to provide closed-loop robustness and represent noise in the system. In Figure 2, the weight Wn is a diagonal matrix with one entry for each of the plant outputs. The selection of the individual noise weights is typically performed selecting an acceptable level of noise and frequency range for each channel (based on the type of sensor and measurement). Care must be exercised not to select a level of noise too high for the system in order to avoid degraded performance objectives. For example, for the flight path angle, which typically for a jumbo jet as the Boeing 747-100/200 is close to zero degrees, a constant level of noise corresponding to 0.01 degrees is used. On the other hand, the altitude, velocity and normal acceleration noise weights are selected as first order weights with the bandwidth depending on the characteristics of the measurement (very slow for altitude and faster dynamics for the velocity and acceleration) and a chosen level of noise in tune with their corresponding values.

$$Wn_{\gamma} = \frac{0.01}{57.3} \qquad Wn_{\dot{V}} = 0.1\frac{\frac{s}{0.5}+1}{\frac{s}{100}+1} \tag{14}$$

$$Wn_{\theta} = \frac{0.05}{57.3} \qquad Wn_{q} = \frac{0.01}{57.3} \tag{15}$$

$$Wn_{Vtas} = 0.05\frac{\frac{s}{0.5}+1}{\frac{s}{100}+1} \qquad Wn_{he} = \frac{\frac{s}{0.01}+1}{\frac{s}{150}+1} \tag{16}$$

V. Integrated Controller/Filter Analysis

Five LTI $\mathcal{H}_\infty$ integrated controllers are synthesized (corresponding to the five equilibrium points from Table 1). An $\mathcal{H}_\infty$-norm of 1.4142 is obtained for all the designs. The controllers have 20 states, 7 inputs, and 4 outputs. In cases where the order of the controller is such that it becomes an issue for implementation there are several techniques available to reduce it (e.g. Hankel state reduction, model truncation, ...). In this case no effort was made to reduce the controller since hardware-in-the-loop was not attempted. For brevity, only the analysis of the controller designed at the nominal design point, point 1 ($he = 4000$ meters, $Vtas = 184$ meters/seconds), is presented in this section.

It is well-known that $\mathcal{H}_\infty$ techniques have no guarantees with respect to the stability of the controller. An unstable controller could also stabilize the closed-loop system but for practical reasons is not acceptable, hence the stability of the controllers is checked and found satisfactory. Furthermore, $\mathcal{H}_\infty$ controllers tend to have very fast poles (tending to infinity for the optimal case) which slow down the time-domain simulations thus residualization is sometimes used. In the present case there is no need since the fastest pole of the controller is around 50 radians/seconds.

In Figure 3, the sensitivity S and complementary sensitivity T functions for the control and diagnosis channels are shown. From left to right and top to bottom the following transfer functions are plotted: $\gamma_{cmd}, Vtas_{cmd}$, actuator fault f_{act}, and sensor fault f_{sen} (each to their respective output and error). The plots show very good results for T and S (i.e. the sum of their magnitudes is about one, $T + S = 1$, and the magnitude is one at frequencies below cross-over for T and one at frequencies above it for S). No remarkable coupling between the two commands is observed. The only exception is a small peak of the $Vtas_{cmd}$ on the γ_{error} but at relatively high frequency compared to the γ bandwidth. Since the velocity is considered a very slow state[26] this coupling is considered negligible.

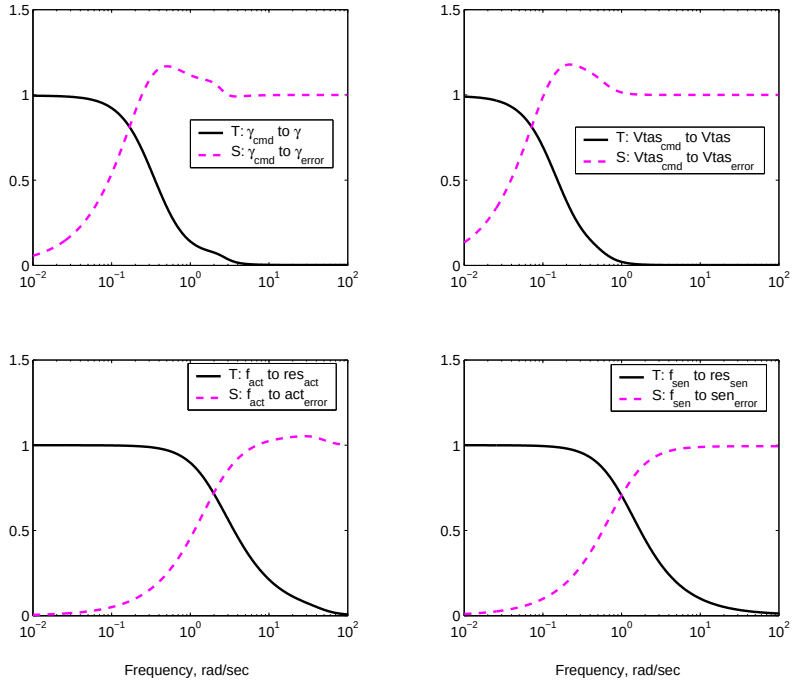

Figure 3. Unweighted closed-loop system: T and S.

From past experience with this system and a similar controller / filter set-up, see references,[22,25] it is expected that the residual channels will have some level of coupling (predominantly in the actuator residual). Figure 4 shows the unweighted interconnection transfer functions of the main channels that result in coupling on the fault residuals. The top plot is for the elevator fault residual res_{act}, and the bottom plot for the sensor residual res_{sen}. It is observed that as expected, the θ channel results in coupling on both fault residuals, observe $TF_{\theta \to res_{act}}$ vs $TF_{f_{act} \to res_{act}}$ and $TF_{\theta \to res_{sen}}$ vs $TF_{f_{sen} \to res_{sen}}$, although with a higher gain (and hence influence) for the actuator residual.

The actuator residual also suffers coupling due to the sensor fault, $TF_{f_{sen} \to res_{act}}$, the flight path command, $TF_{\gamma_{cmd} \to res_{act}}$, and from the pitch rate transfer function, $TF_{q \to res_{act}}$ (the latter frequency response is identical to that of the sensor fault $TF_{f_{sen} \to res_{act}}$). The high frequency coupling from q will be shown later to have adverse consequences for incipient (small) actuator fault diagnosis. With respect to the sensor residual transfer functions, the pitch rate to the sensor residual transfer function, $TF_{q \to res_{sen}}$, is also identical to that from the sensor fault, $TF_{f_{sen} \to res_{sen}}$. This is expected as

the sensor fault enters in additive manner through the pitch rate channel, but it also means that actuator faults affecting the pitch rate will also show up on the sensor residual (although small since the coupling between the residuals is very small). No other noticeable coupling is observed for the sensor residual.

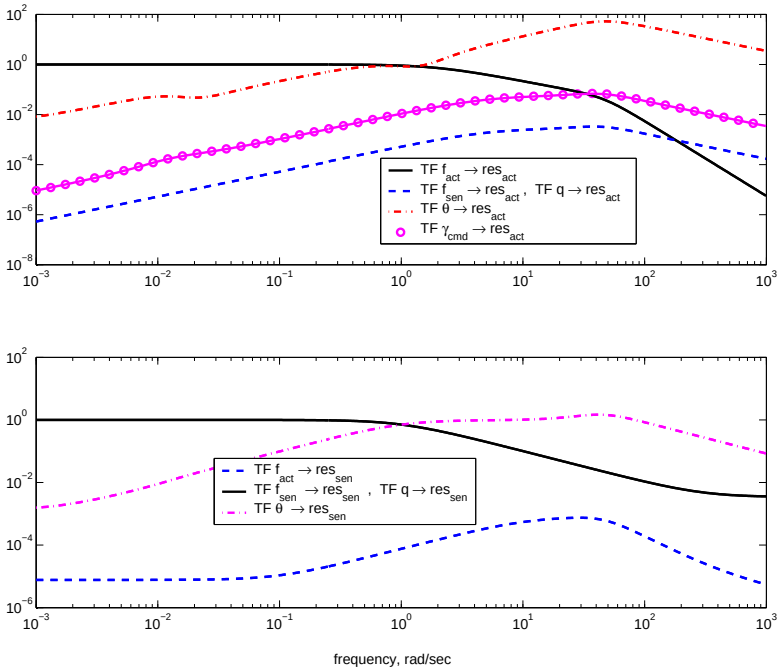

Figure 4. Transfer functions disturbances and commands to residuals.

A. Time Simulations.

The final evaluation of the integrated controller / filter is carried out using linear and nonlinear time simulations. For the LTI simulations the commands to the controller are a -2 deg γ_{cmd} square input from $t = 15$ to $t = 60$ sec, and a square $Vtas$ command of 15 m/s starting at $t = 16$ and ending at $t = 130$ sec. The faults are clearly shown in Figure 5 by the dashed line, they correspond to 50 to 140 percent the actuator magnitude (e.g. a nominal deflection of 1 degree will suffer and additive fault of 1.4 degrees) under a no-fault simulation and up to 300 percent for the sensor fault. This convoluted set of fault inputs is introduced in order to analyze couplings between the faults and the commands. It is unlikely a fault behaviour like this will happen in the real system.

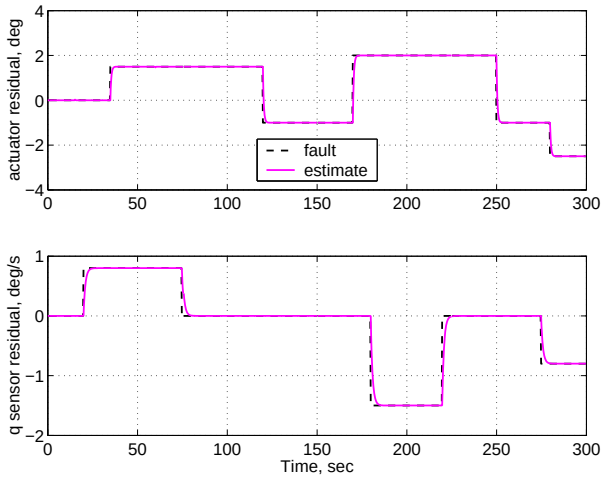

Figure 5. Residuals - LTI closed-loop integrated control.

Figures 5 and 6 show the fault residuals, the plant responses, and the plant inputs for the LTI closed-loop simulation for the nominal -point 1- plant of the $\mathcal{H}_\infty$ integrated controllers (results are almost the same for all the designs).

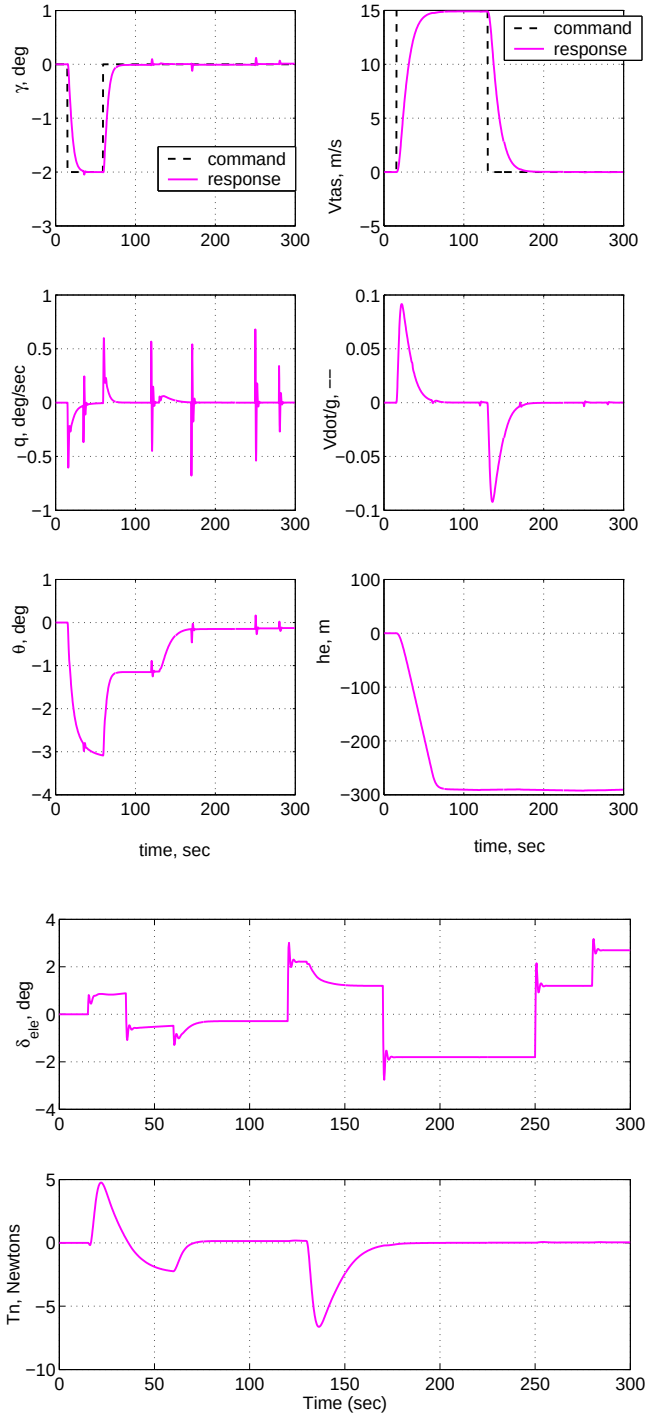

Figure 6. Plant responses and inputs - LTI closed-loop integrated control.

It is observed from the figures that the fault estimation and the command tracking are very good. The detection time (settling-time for the diagnosis) is about 3 and 4 seconds for the actuator and sensor faults respectively. No remarkable coupling is appreciated in either of the fault signals, hence the decoupling objective for the fault estimates is achieved in the LTI case. The settling times for the commands are 20 seconds for the γ command, and 40 seconds approximately for the velocity (by design they were selected to be around 15 and 45 seconds respectively). The

velocity is more robust, with respect to the faults, than the γ channel. The actuator fault is observed to produce coupling in γ although very small, i.e. fast transient with a magnitude of 0.1 degrees for almost a 3 degree abrupt fault in the elevator. This coupling becomes obvious looking at the pitch rate, pitch angle, and the elevator responses. It is the result of undesirable behaviour introduced by the faults that the controller tries to reject. Indeed from the study of the pitch rate plot in Figure 6, it is noted that the first and third peaks (from the left) are caused by the γ command while all the others are due to the elevator faults. The peaks due to the elevator fault are also observed in the θ channel which is used to provide the gamma tracking. This means that faults will show up initially in the elevator, directly affecting the pitch rate q and angle θ; subsequently, the controller would react to ameliorate their effects.

The next step is to simulate the integrated controllers in the nonlinear closed loop. Closing the loop with the nonlinear system enables evaluation of the LTI designs for robustness to model uncertainty. Furthermore, in order to analyze the behaviour of the different $\mathcal{H}_\infty$ designs, Figure 7 shows the nonlinear closed-loop residual and command responses without gust or noise for the nominal design flight condition, point 1, and two other extreme flight conditions, points 3 and 5. The manoeuvre selected is a steadily accelerated climb performed by commanding a 3 degree square command for the flight path angle γ_{cmd} from $t = 15$ to $t = 95$, and a velocity step command of 18 m/s starting at time $= 20$ seconds. This results in a flight profile that takes the aircraft sufficiently away from the design equilibrium point in order to facilitate evaluation of the neighborhood around which the LTI designs are valid.

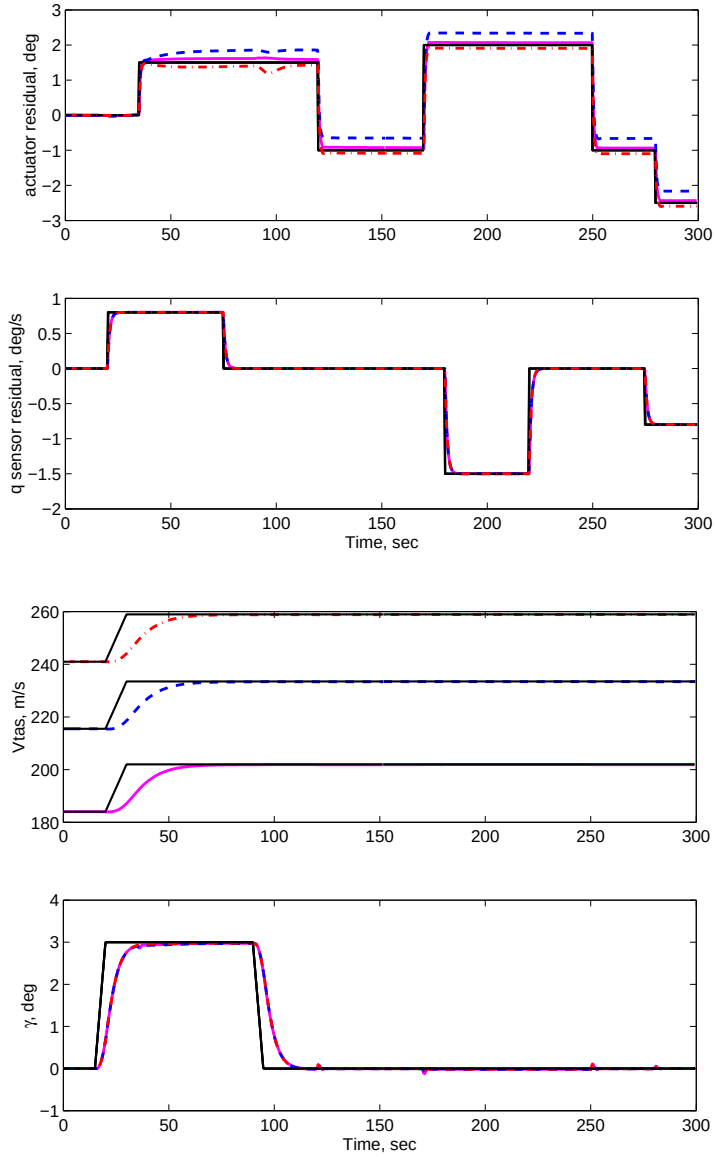

Figure 7. Nonlinear simulation: control commands (thin solid), points 1 (thick solid), 3 (thick dashed), 5 (thick dashed-dot).

It is observed that for the sensor residual the three $\mathcal{H}_\infty$ LTI designs show exactly the same characteristics. The actuator residual is less robust with different levels of steady-state errors for each of the designs. The nominal flight condition ($he = 4000m, Vtas = 184m/s$) is given by the thick solid line and has been analyzed before; flight condition 3 ($he = 9250m, Vtas = 125m/s$) is given by the thick dashed line and shows the largest error, approximately 25-30 percent of constant bias; the last flight condition, point 5 ($he = 7000m, Vtas = 241m/s$) is given by the dashed dot line and shows an error similar to the nominal flight condition but slightly more transient influence by the γ_{cmd}. The command responses show almost identical type of behaviour for all the designs. These results mean that the designs are all very robust to plant variations with only the actuator residual requiring minor corrections as the altitude and velocity change, possibly only gain changes scheduled on these two parameters.

The disturbance rejection characteristics of the integrated controller are tested by using the turbulence model and noisy sensors given in Section III. A moderate level of turbulence is also selected ($L_g = 530$ m and $\sigma = 3.84 - he$ 0.000234 m/s). The noise in the sensors is accomplished by feeding white noise with the corresponding output noise power to the respective sensor. The design flight condition number 5 is used for the noisy closed-loop nonlinear time simulations.

Figure 8 shows the fault residuals under this noisy environment. As expected the sensor residual does a better job rejecting the disturbances, while the actuator residual is more sensitive. Nevertheless, the actuator residual unmistakably diagnoses the elevator fault. The level of noise present in the actuator residual, $\pm$ 0.2 degrees, might prevent the detection of small incipient elevator faults but these faults are not critical at that level (the elevator limits are +17/-23 degrees). In any case, a residual evaluation stage could suffice to provide a more desirable level of incipient fault detection.

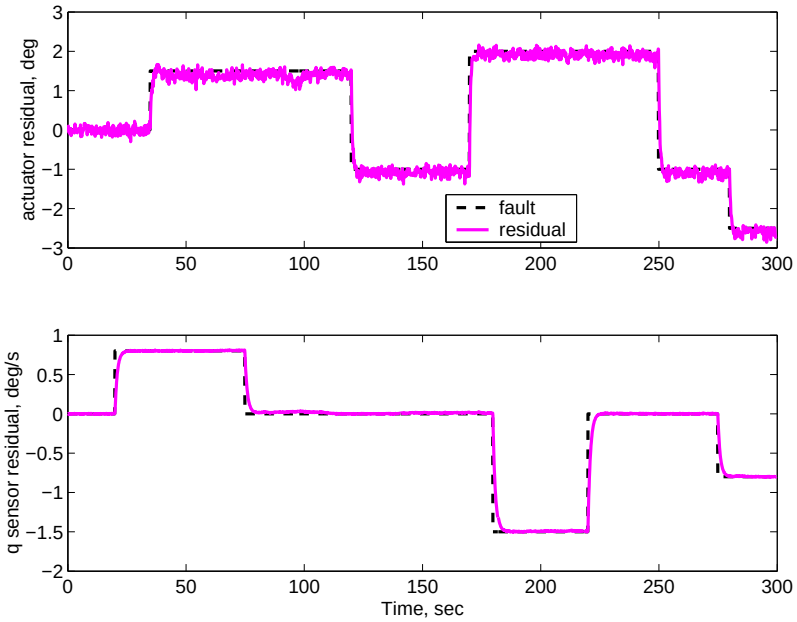

Figure 8. Residuals - Nonlinear closed loop, moderate gust/noise (flight condition 5).

Figure 9 shows the corresponding plant inputs and outputs. Very good disturbance rejection is observed for the commands. The pitch rate angle shows high frequency effects due to the noise, a level of $\pm$ 0.2 degrees. These effects are acceptable for this channel, but it is noted that they are reflected also in the elevator channel and by the coupling of q on the actuator residual they are transmitted to the actuator residual resulting in the afore mentioned level of missed incipient faults.

B. Additional Fault Cases.

Two more fault cases are used to analyze the robustness and performance of the integrated controller under severe faults in the elevator actuator (case 2), and drifts on the actuator and sensor (case 3). Both fault cases are shown for the nominal design point 1 and the same flight profile and moderate level of turbulence and noise as in the last case is used.

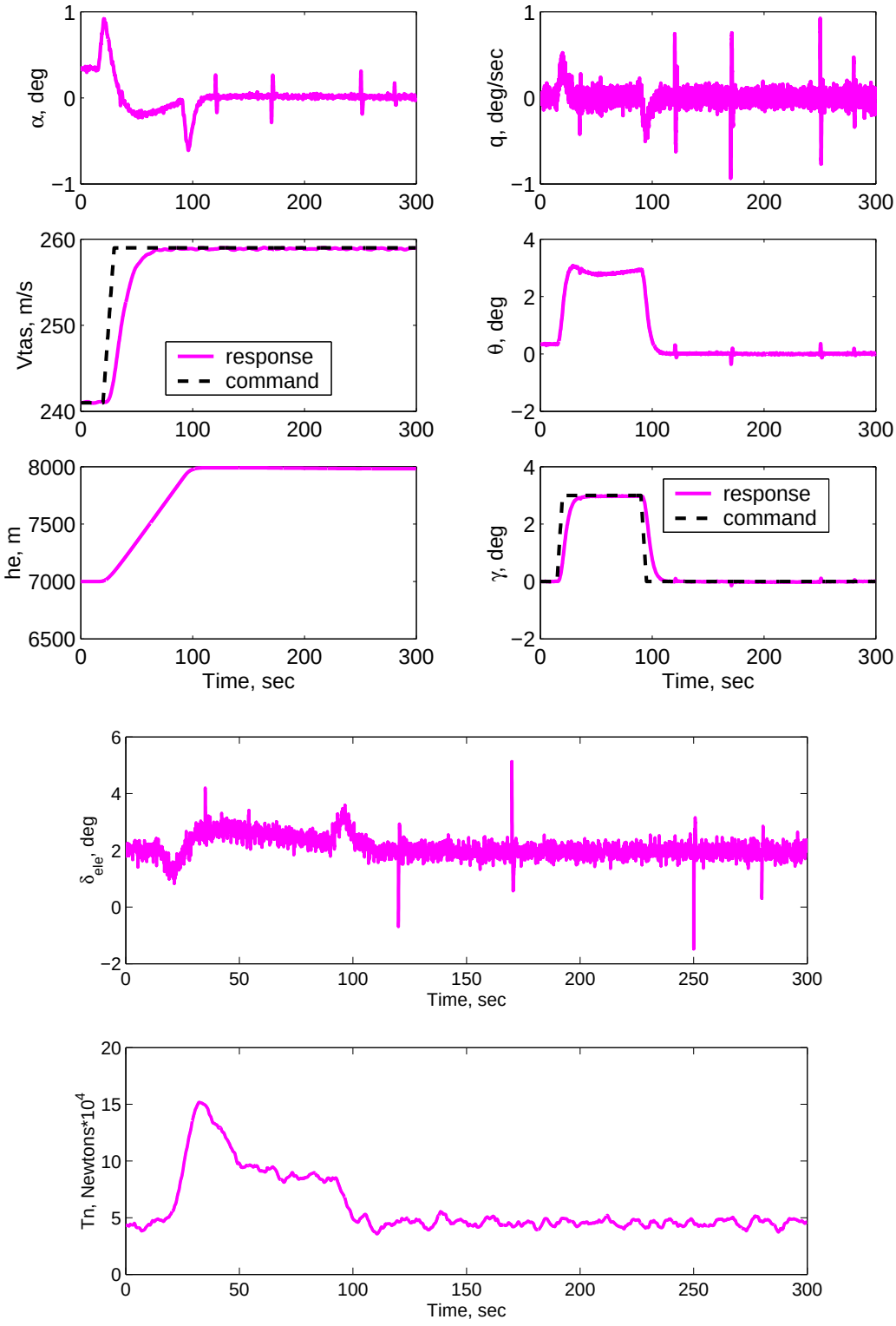

Figure 9. Plant responses and inputs - Nonlinear closed-loop, moderate gust/noise (flight condition 5).

The second fault case represents a severe malfunction of the actuator for the elevator, specifically a 90 percent loss. The same sensor fault as before is used. The actuator fault is obtained by multiplying the output of the actuator with a gain of 0.1, the fault signal is derived by subtracting the deflections before and after the gain. It is expected that the γ

tracking performance will degrade since the elevator controls this tracking objective (although it will be seen that the controller is robust enough to maintain fly-ability).

Figures 10 and 11 show the residuals and the plant outputs. The sensor residual shows the good robustness and performance obtained before for sensor fault diagnosis. The actuator fault residual also does a very good job of diagnosing the fault, note the very large magnitude of the fault. The introduction of the fault is instantaneous (the Simulink block diagram contains the 0.1 gain as the simulation is started) but the aircraft is initialized at the no-fault flight condition. This leads to the initial jump from zero to -20 degrees in the actuator residual. It is noted that the design requirement was to identify faults in the actuator, a supervisory module should be added if it is also desirable to exactly classify the fault as a 90 percent malfunction.

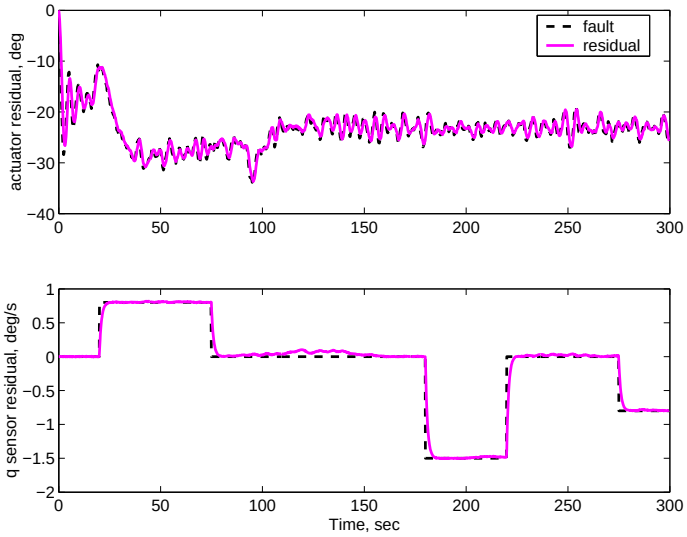

Figure 10. Residuals - Nonlinear closed loop, moderate gust/noise fault case 2.

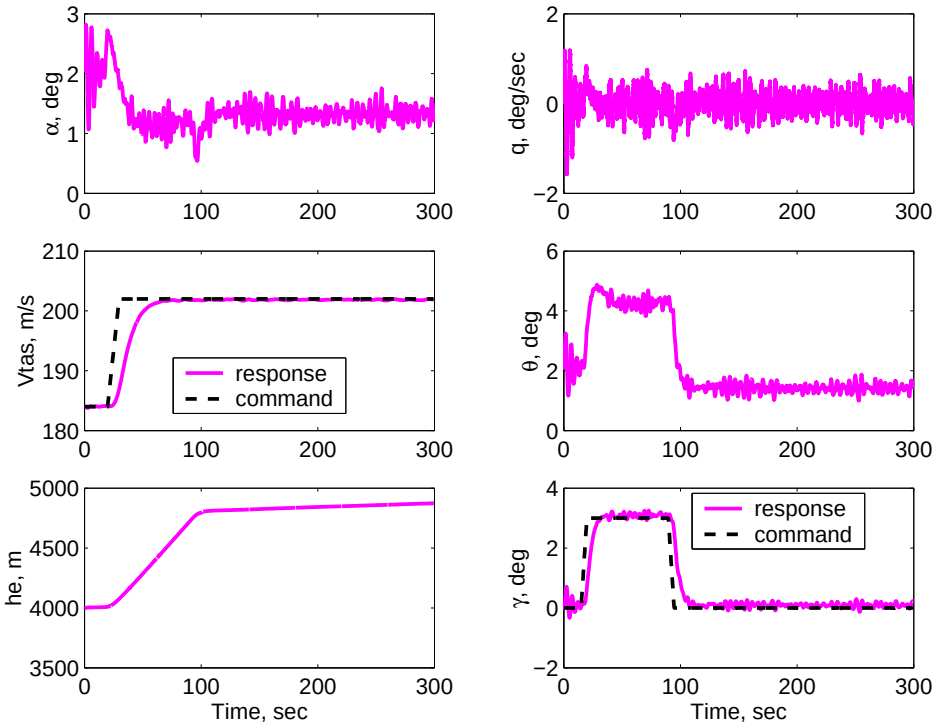

Figure 11. Plant responses - Nonlinear closed loop, moderate gust/noise fault case 2.

Looking at Figure 11 it is observed that the velocity tracking is not affected by the actuator fault nor the sensor fault (again highlighting the good de-coupling for this channel). The difference in the initialization of the simulation is observed in all those channels dependent on the elevator $(\gamma, \theta, q, \alpha)$. The performance of the flight path angle γ is of course affected although not at the severity that would have been expected for a fault of this magnitude. Indeed, under the severity of the fault the controller does a commendable job providing good performance and robustness.

The third fault case assumes faults in the actuator and sensor with an initial drift followed by a constant bias (both added to the nominal deflection). The drift section enables the evaluation of the integral effect of the controller for ramp-type faults. Only the residual and commands results are shown, see Figure 12. Conclusions similar to those for the previous cases are obtained: the actuator residual suffers of a certain degraded disturbance rejection but it identifies the fault quite well. The sensor residual identifies the fault and rejects all other influences very well. The tracking objectives are perfectly satisfied.

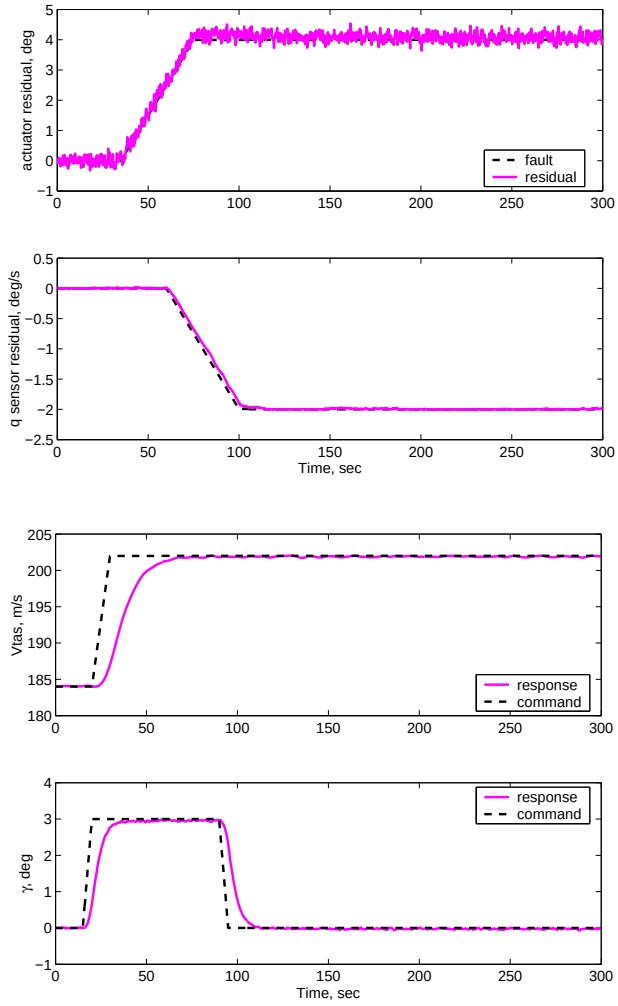

Figure 12. Commands - Nonlinear closed loop, moderate gust/noise fault case 3.

VI. Conclusions

In this paper an application of the integrated controller / diagnosis filter using $\mathcal{H}_\infty$-optimization has been presented for the longitudinal motion of a Boeing 747-100/200 aircraft. Several integrated controllers were synthesized using LTI plants at different flight conditions. The $\mathcal{H}_\infty$ LTI integrated controllers were validated through time simulations using a nonlinear model of the aircraft. The results show that the integrated design has good performance and robustness characteristics for the control and diagnosis objectives. Furthermore, the integrated design allows for fault tolerant control objectives by directly accounting for the faults in the problem formulation.

VII. Acknowledgments

This research was supported under NASA Langley Cooperative Agreement No. NCC-1-337, technical contract monitor Dr. Christine Belcastro.

References

[1]Nett, C.N., Jacobson, C.A., and Miller, A.T., "An Integrated Approach to Controls and Diagnostics: the 4-Parameter Controller," *American Control Conference*, 1988, pp. 824–835.

[2]Stoustrup, J., Grimble, M.J., and Niemann, H., "Design of Integrated Systems for the Control and Detection of Actuator/Sensor Faults," *Sensor Review*, Vol. 17 (2), July 1997, pp. 138–149.

[3]Wu, N.E., "Robust Feedback Design with Optimized Diagnostic Performance," *IEEE Transactions on Automatic Control*, Vol. 42, No. 9, Sept 1997, pp. 1264 –1268.

[4]Tyler, M.L. and Morari, M., "Optimal and Robust Design of Integrated Control and Diagnostic Modules," *American Control Conference*, Baltimore, MD, June 1994, pp. 2060–2064.

[5]Zhou, K., Doyle, J.C., and Glover, K., *Robust and Optimal Control*, Prenticel-Hall, Englewood Cliffs, NJ, 1996.

[6]Tay, T.T., Mareels, I., and Moore, J.B., *High Performance Control*, Birkhauser, 1998.

[7]Suzuki, T. and Tomizuka, M., "Joint Synthesis of Fault Detector and Controller Based on Structure of Two-Degree-of-Freedom Control System," *IEEE Conference on Decision and Control*, Phoenix, AZ, Aug 1999, pp. 3599–3604.

[8]Stoustrup, J. and Niemann, H., "Fault Tolerant Feedback Control," *ECC, Porto, Portugal*, Sept. 2001, pp. 1970–1974.

[9]Zhou, K. and Ren, Z., "A New Controller Architecture for High Performance, Robust, and Fault-Tolerant Control," *IEEE Transactions on Automatic Control*, Vol. 46, No. 10, 2001, pp. 1613–1618.

[10]Nett, C.N., "Algebraic aspects of linear control system stability," *IEEE Transactions on Automatic Control*, Vol. 31, No. 10, Oct 1986, pp. 941–949.

[11]Marcos, A., *Aircraft Applications of Fault Detection and Isolation Techniques*, Ph.D. thesis, Department of Aerospace Engineering and Mechanics, University of Minnesota-Minneapolis, Minneapolis,MN, February 2004.

[12]Ding, X. and Frank, P.M., "Fault Detection via Factorization Approach," *Systems and Control Letters*, Vol. 14, 1990, pp. 431–436.

[13]Ding, X. and Frank, P.M., "An Approach to Robust Residual Generation and Evaluation," *IEEE Conference on Decision and Control*, Brighton, England, December 1991.

[14]Chen, J. and Patton, R.J., *Robust Model-Based Fault Diagnosis for Dynamic Systems*, Kluwer Academic Publishers, 1999.

[15]Vidyasagar, M., *Control System Synthesis: A Factorization Approach*, MIT Press, Cambridge, Massachusetts, 1985.

[16]Niemann, H. and Stoustrup, J., "Integration of Control and Fault Detection: Nominal and Robust Design," *IFAC Safeprocess '97*, Hull, UK, Aug. 1997, pp. 341–346.

[17]Niemann, H. and Stoustrup, J., "Robust Fault Detection in Open Loop vs. Closed Loop," *36th IEEE Conference on Decision and Control*, San Diego, California, Dec. 1997, pp. 4496–4497.

[18]Marcos, A., *A Linear Parameter Varying Model of the Boeing 747-100/200 Longitudinal Motion*, Master's thesis, Department of Aerospace and Engineering Mechanics, University of Minnesota, 2001.

[19]Marcos, A. and Balas, G.J., "Linear Parameter Varying Modeling of the Boeing 747-100/200 Longitudinal Motion," *AIAA Guidance, Navigation, and Control Conference, AIAA-2001-4347*, Montreal, Canada, August 2001.

[20]Etkin, B. and Reid, L., *Dynamics of Flight Stability and Control*, John Wiley and Sons Inc., 1996.

[21]Stevens, B. and Lewis, F., *Aircraft Control and Simulation*, John Wiley & Sons, Inc., 2nd ed., 1992.

[22]Marcos, A., Ganguli, S., and Balas, G.J., "Application of $\mathcal{H}_\infty$ Fault Detection and Isolation to a Boeing 747-100/200 Aircraft," *AIAA Guidance, Navigation, and Control Conference, AIAA-2002-4944*, Monterey, CA, August 2002.

[23]Hanke, C. and Nordwall, D., " The Simulation of a Jumbo Jet Transport Aircraft. Volume II: Modeling Data," Tech. Rep. NASA CR-114494/D6-30643-VOL-2, The Boeing Company, 1970.

[24]Mulder, J.A. and van der Vaart, J.C., "Aircraft Responses to Atmospheric Turbulence," Tech. Rep. Lectures Notes D-4, Delft University of Technology, Delft, The Netherlands, 1998.

[25]Ganguli, S., Marcos, A., and Balas, G.J., "Reconfigurable LPV Control Design for Boeing 747-100/200 Longitudinal Axis," *American Control Conference*, Vol. 5, Anchorage, AK, May 2002, pp. 3612 –3617.

[26]Snell, S.A., Enns, D.F., and Garrard, W., "Nonlinear Inversion Flight Control of a Supermaneuverable Aircraft," *Journal of Guidance, Control, and Dynamics*, Vol. 15, No. 4, 1992.